

¹³C ISOTOPIC FRACTIONATION OF HC₃N IN STAR-FORMING REGIONS
- LOW-MASS STAR FORMING REGION L1527 AND HIGH-MASS STAR FORMING REGION G28.28-0.36 -

KOTOMI TANIGUCHI^{1,2}, MASAO SAITO²

Department of Astronomical Science, School of Physical Science, SOKENDAI (The Graduate University for Advanced Studies), Osawa,
Mitaka, Tokyo 181-8588, Japan

HIROYUKI OZEKI

Department of Environmental Science, Faculty of Science, Toho University, Miyama, Funabashi, Chiba 274-8510, Japan

¹kotomi.taniguchi@nao.ac.jp

²Nobeyama Radio Observatory, National Astronomical Observatory of Japan, Minamimaki, Minamisaku, Nagano 384-1305, Japan

ABSTRACT

We observed the $J = 9 - 8$ and $10 - 9$ rotational lines of three ¹³C isotopologues of HC₃N in L1527 and G28.28-0.36 with the 45-m radio telescope of the Nobeyama Radio Observatory in order to constrain the main formation mechanisms of HC₃N in each source. The abundance ratios of the three ¹³C isotopologues of HC₃N are found to be $0.9 (\pm 0.2) : 1.00 : 1.29 (\pm 0.19) (1\sigma)$ and $1.0 (\pm 0.2) : 1.00 : 1.47 (\pm 0.17) (1\sigma)$ for $[\text{H}^{13}\text{CCCN}] : [\text{HC}^{13}\text{CCN}] : [\text{HCC}^{13}\text{CN}]$ in L1527 and G28.28-0.36, respectively. We recognize a similar ¹³C isotopic fractionation pattern that the abundances of H¹³CCCN and HC¹³CCN are comparable, and HCC¹³CN is more abundant than the others. Based on the results, we discuss the main formation pathway of HC₃N. The ¹³C isotopic fractionation pattern derived from our observations can be explained by the neutral-neutral reaction between C₂H₂ and CN in both the low-mass (L1527) and high-mass (G28.28-0.36) star forming regions.

Keywords: astrochemistry — ISM:individual objects (L1527, G28.28-0.36) — ISM:molecules — stars:formation

1. INTRODUCTION

Almost 200 molecules have been detected in the interstellar medium or circumstellar shells so far. In dark clouds, unsaturated carbon-chain molecules such as CCS are abundant, whereas they decrease in star forming cores (Suzuki et al. 1992). These carbon-chain molecules are formed from C or C⁺ in the gas phase before carbon atoms are converted into CO. On the other hand, saturated complex organic molecules such as CH₃OH and CH₃CN increase in star forming regions, and these regions are called hot cores for high-mass star forming regions and hot corinos for low-mass star forming regions. In hot cores and hot corinos, the combination between grain-surface reactions and gas-phase reactions produces various saturated complex organic molecules (e.g. Garrod & Herbst 2006).

Recently, in contrast to the above scenarios, several star forming cores associated with carbon-chain molecules have been discovered. Sakai et al. (2008) showed that various carbon-chain molecules are abundant toward the low-mass star forming region L1527. Several chemical model calculations showed that CH₄ plays an essential role in efficient formation of carbon-chain molecules in the warm regions (≥ 25 K) (e.g. Aikawa et al. 2008; Hassel et al. 2008). Aikawa et al. (2008) indicated that carbon-chain molecules are formed by a combination of gas-phase reactions and grain-surface reactions following the sublimation of CH₄. These low-mass star forming regions were named Warm Carbon Chain Chemistry (WCCC) sources.

Cyanopolyynes (HC_{2n+1}N) are one of the representative carbon-chain-molecule series. Hassel et al. (2008) demonstrated that regeneration of carbon-chain molecules results from gas-phase chemistry and showed the primary formation pathway of HC₃N as follows:



Chapman et al. (2009) presented their time-dependent gas-phase chemical model and showed that cyanopolyynes (HC_{2n+1}N ; $n = 1 - 4$) can be formed under hot core conditions. They considered that C_2H_2 is released from the grain mantle inside hot cores and the neutral-neutral reaction between C_2H_2 and CN (Reaction (1)) proceeds relatively easily for the hot core temperature (100 – 300 K). Their chemical model calculation was supported by detections of HC_5N toward 35 hot cores associated with 6.7 GHz methanol masers (Green et al. 2014). Therefore, the predicted main formation pathway of HC_3N is Reaction (1) in both the low-mass star forming region L1527 and the high-mass star forming regions.

Deriving ^{13}C isotopic fractionation of carbon-chain molecules by observations is one of the promising methods to constrain their main formation mechanism. For example, the dominant formation mechanism of HC_3N has been investigated based on its ^{13}C isotopic fractionation (Takano et al. 1998) toward the cyanopolyne peak in Taurus Molecular Cloud-1 (TMC-1 CP; $d = 140$ pc). The derived abundance ratios of three ^{13}C isotopologues of HC_3N are $[\text{H}^{13}\text{CCCN}] : [\text{HC}^{13}\text{CCN}] : [\text{HCC}^{13}\text{CN}] = 1.0 : 1.0 : 1.4 (\pm 0.2) (1\sigma)$, and it is suggested that its main formation pathway is the neutral-neutral reaction between C_2H_2 and CN (Takano et al. 1998). Thus investigation of formation mechanism of HC_3N using its ^{13}C isotopic fractionation has proved successful.

In the present paper, we observed the three ^{13}C isotopologues of HC_3N , the shortest cyanopolyne, toward L1527 ($d = 140$ pc) and G28.28-0.36 ($d = 3.0$ kpc, Green et al. (2014)) with the 45-m radio telescope of the Nobeyama Radio Observatory (NRO) in order to compare ^{13}C isotopic fractionation of HC_3N and its main formation mechanisms in the two star forming regions. G28.28-0.36 is one of the hot cores that Green et al. (2014) detected HC_5N , and associates with an ultra compact HII region. Purcell et al. (2006) detected CH_3CN , a hot core tracer, and H^{13}CO^+ toward the hot core.

2. OBSERVATIONS

We carried out observations of the three ^{13}C isotopologues of HC_3N (H^{13}CCCN , HC^{13}CCN , and HCC^{13}CN) simultaneously with the NRO 45-m radio telescope in 2015 December, 2016 February, March and April (2015-2016 season). We also observed the normal species of the $J = 9 - 8$ rotational lines simultaneously, when we observed the $J = 9 - 8$ lines of the three ^{13}C isotopologues. We used the TZ and the T70 receivers for the observations of the $J = 9 - 8$ transition lines, and the TZ receiver for the observations of the $J = 10 - 9$ transition lines. We used the TZ receiver for the observations of the $J = 9 - 8$ lines, after we could not use the T70 receiver due to equipment troubles. The rest frequencies of the observed lines are given in Table 2. Both receivers allow us to obtain dual-polarization data simultaneously. The beam sizes (HPBW) and main beam efficiencies (η_B) were 18" and 54% for the TZ receiver and 20" and 56% for the T70 receiver at 86 GHz, respectively. The system temperatures were between 120 and 250 K, depending on the weather conditions and the elevations. We employed the position-switching mode.

The observed position and off-source position for L1527 were $(\alpha_{2000}, \delta_{2000}) = (04^{\text{h}}39^{\text{m}}53^{\text{s}}.89, 26^{\circ}03'11''.0)$ and $(04^{\text{h}}42^{\text{m}}35^{\text{s}}.9, 25^{\circ}53'23''.3)$, respectively. The telescope pointing was checked using the H40 receiver every 1.5 hours by observing the SiO maser line ($J = 1 - 0$) from NML Tau, and the pointing error was less than 3". The observed position for G28.28-0.36 was $(\alpha_{2000}, \delta_{2000}) = (18^{\text{h}}44^{\text{m}}13^{\text{s}}.3, -04^{\circ}18'03''.3)$, and the off-source position was set to be +15' away in the declination. We checked the pointing accuracy by observing the SiO maser lines ($J = 1 - 0$) from OH39.7+1.5 every 1 – 1.5 hours, depending on the wind conditions. The pointing error was within 3". We used the SAM45 FX-type digital correlator in frequency settings whose bandwidths and resolutions are 125 MHz and 30.52 kHz, and 250 MHz and 61.04 kHz for L1527 and G28.28-0.36, respectively. We applied 2 channel binding, and velocity resolutions of final spectra are 0.25 and 0.5 km s^{-1} for L1527 and G28.28-0.36, respectively.

3. RESULTS AND ANALYSIS

3.1. Results

The spectra of the three ^{13}C isotopologues of HC_3N were taken with signal-to-noise ratios of 6.3 – 10.6 in L1527, except the $J = 10 - 9$ line of H^{13}CCCN , as shown in Figure 1. We also show the spectra of the $J = 9 - 8$ rotational line of the normal species observed with its ^{13}C isotopologues simultaneously. The values of V_{LSR} are in good agreement with the V_{LSR} value reported for this source (5.9 km s^{-1}). We derived their integrated intensities with the same velocity range, and the results are summarized in Table 1. The ratios of the integrated intensities among the three ^{13}C isotopologues of the $J = 10 - 9$ lines are consistent with those of the $J = 9 - 8$ lines. However, we cannot detect H^{13}CCCN using the $J = 10 - 9$ line with signal-to-noise ratio above 3, and we do not use the $J = 10 - 9$ lines in the following analyses. We evaluated the error of the integrated intensities using the following formula:

$$\Delta T_{\text{A}}^* (\text{K}) \times \sqrt{n} (\text{ch}) \times v (\text{km s}^{-1}) \quad (2)$$

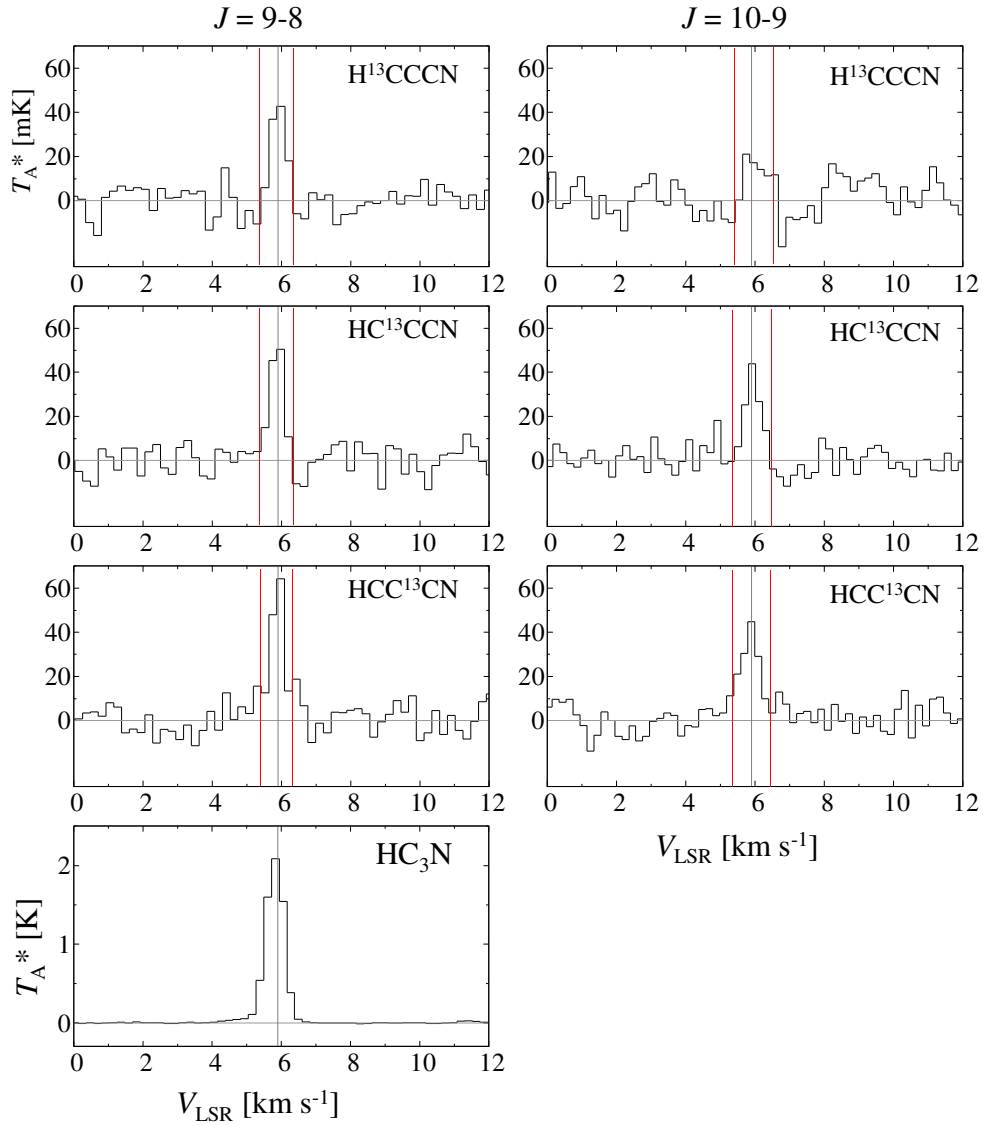


Figure 1. The spectra of the three ^{13}C isotopologues of HC_3N of the $J = 9 - 8$ and $J = 10 - 9$ rotational transitions and the normal species of the $J = 9 - 8$ rotational transition toward L1527. The gray vertical lines show $V_{\text{LSR}} = 5.9 \text{ km s}^{-1}$. The red vertical lines show the range using for the integrated intensities.

In Equation (2), ΔT_{A}^* is the rms noises in the emission-free regions, n is the numbers of channels, and v is the velocity resolution per channel. The rms noises are summarized in Table 2. We used 4 ch and 0.25 km s^{-1} for n and v , respectively, in L1527.

The three ^{13}C isotopologues of HC_3N were detected with signal-to-noise ratios of $5.1 - 10.7$ in G28.28-0.36, as shown

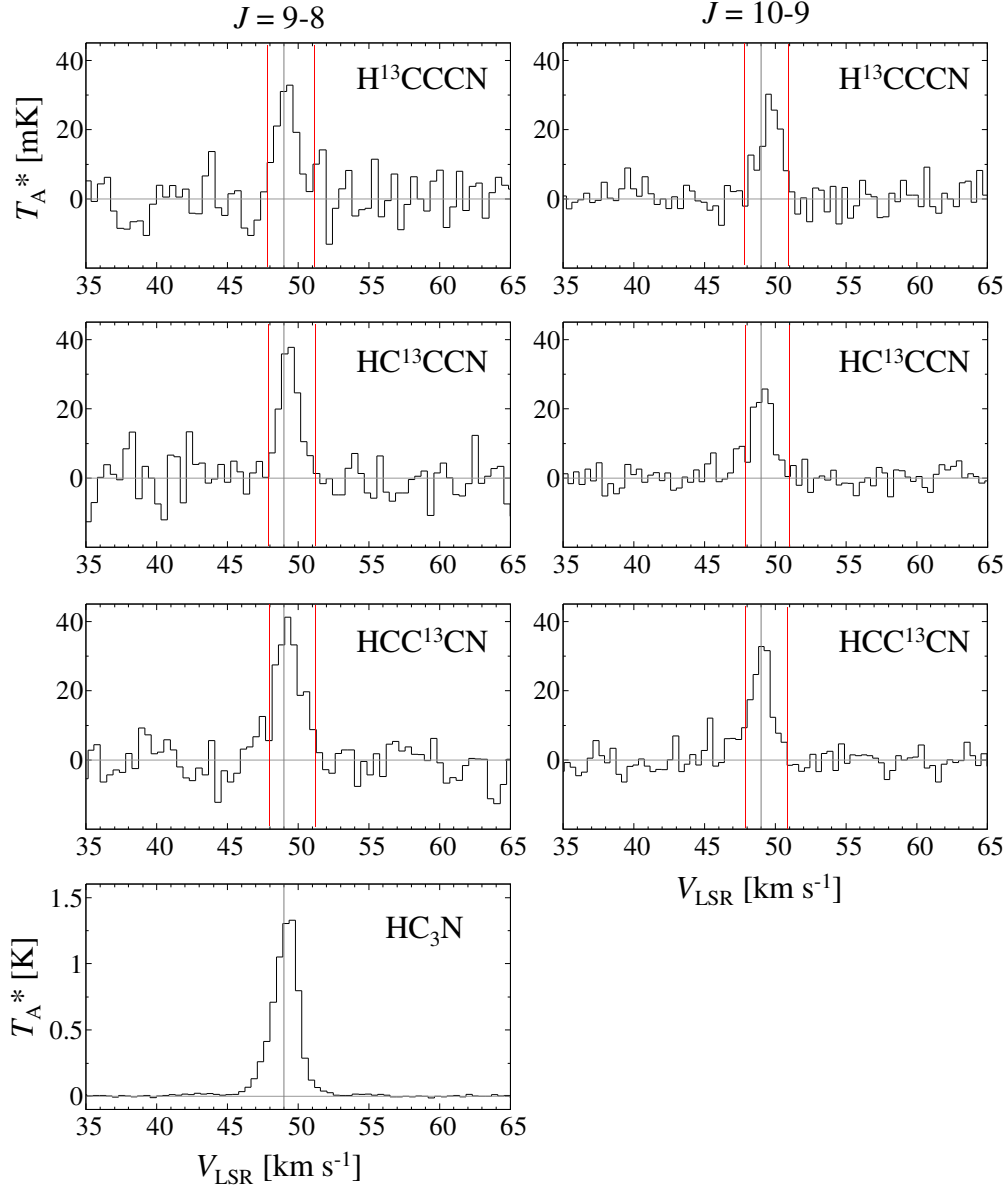


Figure 2. The spectra of the three ^{13}C isotopologues of HC_3N of the $J = 9 - 8$ and $J = 10 - 9$ rotational transitions and the normal species of the $J = 9 - 8$ rotational transition toward G28.28-0.36. The gray vertical lines show $V_{\text{LSR}} = 48.9 \text{ km s}^{-1}$. The red vertical lines show the range using for the integrated intensities.

in Figure 2. The values of V_{LSR} agree with one another and the systematic velocity reported for the source (48.9 km s^{-1} Purcell et al. (2006)). We derived the integrated intensities of the three ^{13}C isotopologues of HC_3N in the same way as L1527, and their errors were calculated using Equation (2) with 7 ch and 0.5 km s^{-1} for n and v , respectively. We summarize the results in Table 1.

Table 1. Integrated Intensities of Three ^{13}C Isotopologues of HC_3N (K km s^{-1})

	H^{13}CCCN	HC^{13}CCN	HCC^{13}CN
L1527			
$J = 9 - 8$	0.021 (3)	0.028 (3)	0.035 (3)
$J = 10 - 9$	0.016 (4)	0.023 (3)	0.032 (3)
G28.28-0.36			
$J = 9 - 8$	0.055 (9)	0.064 (7)	0.090 (7)
$J = 10 - 9$	0.049 (5)	0.047 (4)	0.059 (4)

NOTE—The numbers in parenthesis represent the error values evaluated by Equation (2).

Table 2. Spectral Line Parameters of the Observed Lines

Species	Frequency ^a (GHz)	T_{A}^* (mK)	Δv (km s^{-1})	V_{LSR} (km s^{-1})	rms ^b (mK)
L1527					
$J = 9 - 8$					
HC_3N	81.8814677 (9)	2154 (16)	0.622 (6)	5.8 (3)	5.5
H^{13}CCCN	79.35046 (2)	45 (6)	0.49 (7)	6.0 (3)	6.6
HC^{13}CCN	81.53411 (2)	52 (5)	0.46 (6)	6.0 (3)	5.9
HCC^{13}CN	81.54198 (2)	66 (6)	0.47 (5)	6.0 (3)	6.2
$J = 10 - 9$					
H^{13}CCCN	88.16683 (2)	< 22	-	-	7.4
HC^{13}CCN	90.59306 (2)	43 (5)	0.51 (6)	5.9 (3)	5.9
HCC^{13}CN	90.60178 (2)	39 (4)	0.75 (9)	5.9 (3)	5.9
G28.28-0.36					
$J = 9 - 8$					
HC_3N	81.8814677 (9)	1310 (20)	2.19 (7)	49.2 (5)	6.7
H^{13}CCCN	79.35046 (2)	34 (4)	1.6 (2)	49.4 (5)	6.6
HC^{13}CCN	81.53411 (2)	39 (4)	1.6 (2)	49.5 (5)	5.3
HCC^{13}CN	81.54198 (2)	38 (3)	2.3 (2)	49.3 (5)	5.3
$J = 10 - 9$					
H^{13}CCCN	88.16683 (2)	28 (2)	1.64 (17)	49.5 (5)	3.9
HC^{13}CCN	90.59306 (2)	25 (2)	1.86 (17)	49.3 (5)	2.9
HCC^{13}CN	90.60178 (2)	31 (2)	1.79 (15)	49.0 (5)	2.9

NOTE—The numbers in parenthesis represent one standard deviation in the Gaussian fit except for frequency.

^aTaken from the Cologne Database for Molecular Spectroscopy (CDMS) (Müller et al. 2005).

^bThe rms noises in emission-free regions.

3.2. Analysis

We fitted the spectra with a Gaussian profile and obtained the spectral line parameters, as summarized in Table 2. We calculated the column densities of the normal species and the three ^{13}C isotopologues of HC_3N using the Local Thermodynamic Equilibrium (LTE) analysis as shown in the following formulae (Takano et al. 1998):

$$\tau = -\ln \left[1 - \frac{T_A^*}{f\eta_B \{J(T_{\text{ex}}) - J(T_{\text{bg}})\}} \right], \quad (3)$$

where

$$J(T) = \frac{h\nu}{k} \left\{ \exp\left(\frac{h\nu}{kT}\right) - 1 \right\}^{-1}, \quad (4)$$

and

$$N = \tau \frac{3h\Delta v}{8\pi^3} \sqrt{\frac{\pi}{4\ln 2}} Q \frac{1}{\mu^2} \frac{1}{J_{\text{lower}} + 1} \exp\left(\frac{E_{\text{lower}}}{kT_{\text{ex}}}\right) \left\{ 1 - \exp\left(-\frac{h\nu}{kT_{\text{ex}}}\right) \right\}^{-1}. \quad (5)$$

In Equation (3), T_A^* denotes the antenna temperature, f the beam filling factor, η_B the main beam efficiency, and τ the optical depth. We used 1 and 0.54 for f and η_B (Section 2), respectively. T_{ex} is the excitation temperature, and T_{bg} is the cosmic microwave background temperature ($\simeq 2.7$ K). $J(T)$ in Equation (4) is the Planck function. In Equation (5), N is the column density, Δv is the line width (FWHM), Q is the partition function, μ is the permanent electric dipole moment of HC₃N (3.73172×10^{-18} esu cm, [Deleon & Muentner \(1985\)](#)), and E_{lower} is the energy of the lower rotational energy level.

[Sakai et al. \(2009\)](#) derived the excitation temperatures and the column densities of HC₃N using the LTE analysis. The determined excitation temperatures and column densities are 9.7 ± 0.2 K and $(2.7 \pm 0.2) \times 10^{13}$ cm⁻² when the $J = 5 - 4$ and $J = 10 - 9$ data were included, and 16.9 ± 0.5 K and $(1.19 \pm 0.03) \times 10^{13}$ cm⁻² using only the $J = 10 - 9$ and $J = 17 - 16$ lines. We then derived τ assuming the excitation temperatures of 9.7 K and 16.9 K, respectively, using Equation (3). The calculated column densities are summarized in Table 3. The column densities are determined to be $(2.61 \pm 0.03) \times 10^{13}$, $(2.8 \pm 0.6) \times 10^{11}$, $(3.0 \pm 0.5) \times 10^{11}$, and $(3.9 \pm 0.6) \times 10^{11}$ cm⁻² using the excitation temperature of 9.7 K, and $(7.87 \pm 0.09) \times 10^{12}$, $(1.1 \pm 0.2) \times 10^{11}$, $(1.2 \pm 0.2) \times 10^{11}$, and $(1.5 \pm 0.2) \times 10^{11}$ cm⁻² using the excitation temperature of 16.9 K for HC₃N, H¹³CCCN, HC¹³CCN, and HCC¹³CN, respectively. The two assumed excitation temperatures seem to be the lower and upper limits, and then the derived column densities are also the upper and lower limits. A change in the assumed excitation temperature by a factor of 2 does not affect the derived column densities of the three ¹³C isotopologues within 3-sigma errors. The derived column density of the normal species using the excitation temperature of 9.7 K agrees with that derived by [Sakai et al. \(2009\)](#) ($(2.7 \pm 0.2) \times 10^{13}$ cm⁻²), while the column density using the excitation temperature of 16.9 K is lower than that calculated by [Sakai et al. \(2009\)](#) ($(1.19 \pm 0.03) \times 10^{13}$ cm⁻²) by 1.5 times. The abundance ratios of the three ¹³C isotopologues are derived to be $0.9 (\pm 0.2) : 1.00 : 1.29 (\pm 0.19)$ (1σ) for [H¹³CCCN] : [HC¹³CCN] : [HCC¹³CN].

Using the column densities of the normal species of $(2.7 \pm 0.2) \times 10^{13}$ cm⁻² and $(1.19 \pm 0.03) \times 10^{13}$ cm⁻² for the excitation temperatures of 9.7 K and 16.9 K, respectively ([Sakai et al. 2009](#)), we also calculated the ¹²C/¹³C ratios of HC₃N, as summarized in Table 3. When the excitation temperature is 9.7 K, the ¹²C/¹³C ratios are determined to be 97 ± 21 , 90 ± 15 , and 70 ± 10 (1σ) for H¹³CCCN, HC¹³CCN, and HCC¹³CN, respectively. The ¹²C/¹³C ratios are derived to be 108 ± 23 , 102 ± 18 , and 79 ± 12 (1σ) for H¹³CCCN, HC¹³CCN, and HCC¹³CN, assuming that the excitation temperature is 16.9 K. The ¹²C/¹³C ratios do not change depending on the two assumed excitation temperatures within 1-sigma errors. These ratios would be the lower and upper limits.

We also calculated the column densities of the normal species and the three ¹³C isotopologues of HC₃N in G28.28-0.36, using the $J = 9 - 8$ and $J = 10 - 9$ lines, respectively. We conducted calculations using Equations (3) - (5) with the excitation temperatures of 50, 100, and 200 K, respectively, because the typical temperature in hot cores is ~ 100 K. We summarize the results with the excitation temperature of 100 K in Table 4. The column densities of the normal species and the three ¹³C isotopologues are derived to be $(4.97 \pm 0.18) \times 10^{12}$, $(1.0 \pm 0.2) \times 10^{11}$, $(1.04 \pm 0.17) \times 10^{11}$, and $(1.53 \pm 0.17) \times 10^{11}$ cm⁻² for HC₃N, H¹³CCCN, HC¹³CCN, and HCC¹³CN, respectively, using the $J = 9 - 8$ lines. Using the $J = 10 - 9$ lines, the derived column densities of the three ¹³C isotopologues are $(7.1 \pm 1.0) \times 10^{10}$, $(6.7 \pm 0.8) \times 10^{10}$, and $(8.4 \pm 0.9) \times 10^{10}$ cm⁻² for H¹³CCCN, HC¹³CCN, and HCC¹³CN, respectively. We discuss the differences in the column densities between the $J = 9 - 8$ and $10 - 9$ lines in Section 4.2. The values of the column densities do not change depending on the assumed excitation temperatures within 1-sigma errors. The abundance ratios are found to be $1.0 (\pm 0.2) : 1.00 : 1.47 (\pm 0.17)$ (1σ), and $1.05 (\pm 0.15) : 1.00 : 1.22 (\pm 0.14)$ (1σ) for [H¹³CCCN] : [HC¹³CCN] : [HCC¹³CN] using the $J = 9 - 8$ and $10 - 9$ lines, respectively. Thus the abundance ratios are consistent between the $J = 9 - 8$ and $10 - 9$ lines within 1-sigma errors.

We also derived the ¹²C/¹³C ratios using the $J = 9 - 8$ lines, and these results are summarized in Table 4. The calculated ratios are 50 ± 11 , 48 ± 8 , and 32 ± 4 for H¹³CCCN, HC¹³CCN, and HCC¹³CN, respectively. The ¹²C/¹³C ratios do not change depending on the assumed excitation temperatures.

Table 3. Column Densities and $^{12}\text{C}/^{13}\text{C}$ Ratios of HC_3N in L1527

Species	$T_{\text{ex}} = 9.7 \text{ K}$		$T_{\text{ex}} = 16.9 \text{ K}$	
	Column Density ($\times 10^{11} \text{ cm}^{-2}$)	$^{12}\text{C}/^{13}\text{C}^{\text{a}}$ Ratio	Column Density ($\times 10^{11} \text{ cm}^{-2}$)	$^{12}\text{C}/^{13}\text{C}^{\text{b}}$ Ratio
H^{13}CCCN	2.8 ± 0.6	97 ± 21	1.1 ± 0.2	108 ± 23
HC^{13}CCN	3.0 ± 0.5	90 ± 15	1.2 ± 0.2	102 ± 18
HCC^{13}CN	3.9 ± 0.6	70 ± 10	1.5 ± 0.2	79 ± 12

NOTE—The error corresponds to one standard deviation.

^aThe ratios were derived using the column density of the normal species of $2.7 \pm 0.2 \times 10^{13} \text{ cm}^{-2}$, which was derived by the LTE analysis using $T_{\text{ex}} = 9.7 \text{ K}$ (Sakai et al. 2009).

^bThe ratios were derived using the column density of the normal species of $1.19 \pm 0.03 \times 10^{13} \text{ cm}^{-2}$, which was derived by the LTE analysis using $T_{\text{ex}} = 16.9 \text{ K}$ (Sakai et al. 2009).

Table 4. Column Densities and $^{12}\text{C}/^{13}\text{C}$ Ratios of HC_3N in G28.28-0.36

Species	$J = 9 - 8$		$J = 10 - 9$
	Column Density ($\times 10^{11} \text{ cm}^{-2}$)	$^{12}\text{C}/^{13}\text{C}$ Ratio	Column Density ($\times 10^{10} \text{ cm}^{-2}$)
HC_3N	$(4.97 \pm 0.18) \times 10$	-	-
H^{13}CCCN	1.0 ± 0.2	50 ± 11	7.1 ± 1.0
HC^{13}CCN	1.04 ± 0.17	48 ± 8	6.7 ± 0.8
HCC^{13}CN	1.53 ± 0.17	32 ± 4	8.4 ± 0.9

NOTE—The error corresponds to one standard deviation. The assumed excitation temperature is 100 K.

4. DISCUSSION

4.1. ^{13}C Isotopic Fractionation and Formation Mechanisms of HC_3N

The abundance ratios of the three ^{13}C isotopologues are derived to be $0.9 (\pm 0.2) : 1.00 : 1.29 (\pm 0.19)$ (1σ) and $1.0 (\pm 0.2) : 1.00 : 1.47 (\pm 0.17)$ (1σ) for $[\text{H}^{13}\text{CCCN}] : [\text{HC}^{13}\text{CCN}] : [\text{HCC}^{13}\text{CN}]$ in L1527 and G28.28-0.36, respectively. One possible mechanism producing ^{13}C isotopic fractionation is isotope exchange reactions. As Takano et al. (1998) discussed, the isotope exchange reactions can be negligible in the case of HC_3N . Hence, the differences in the abundances among the three ^{13}C isotopologues should occur during their formation processes.

In both L1527 and G28.28-0.36, the abundance ratios of the three ^{13}C isotopologues of HC_3N show the following two characteristics;

1. The abundances of H^{13}CCCN and HC^{13}CCN are comparable with each other, and
2. The abundance of HCC^{13}CN is higher than the previous two species.

These characteristics imply that the main formation pathway of HC_3N contains two equivalent carbon atoms, and the other carbon atom originates from different parent species. We investigate possible reactions leading to HC_3N , using the UMIST Database for Astrochemistry 2012 (McElroy et al. 2013). The four formation pathways are possible as follows.

Pathway 1: the neutral-neutral reaction between C_2H_2 and CN (Reaction (1)),

Pathway 2: the neutral-neutral reaction between C_2H and HNC ,

Pathway 3: the ion-molecule reactions between C_3H_n^+ ($n = 3-5$) and nitrogen atoms followed by electron recombination reactions, and

Pathway 4: the ion-molecule reactions between C_2H_2^+ and HCN followed by electron recombination reactions.

If Pathway 1 is the main formation pathway of HC_3N , the abundance ratios of the three ^{13}C isotopologues of HC_3N should be $1 : 1 : x$, where x is an arbitrary value, for $[\text{H}^{13}\text{CCCN}] : [\text{HC}^{13}\text{CCN}] : [\text{HCC}^{13}\text{CN}]$, because two carbon atoms in C_2H_2 are equivalent and the triple bond between C and N in CN molecule is preserved during proceeding of the reaction (Fukuzawa & Osamura 1997). Our observational results show $0.9 (\pm 0.2) : 1.00 : 1.29 (\pm 0.19) (1\sigma)$ and $1.0 (\pm 0.2) : 1.0 : 1.47 (\pm 0.17) (1\sigma)$ for $[\text{H}^{13}\text{CCCN}] : [\text{HC}^{13}\text{CCN}] : [\text{HCC}^{13}\text{CN}]$ in L1527 and G28.28-0.36, respectively. Therefore, our observational results are well consistent with the expected ratios by Pathway 1.

In L1527, Hassel et al. (2008) showed the formation pathways leading to C_2H_2 from CH_4 as follows;



followed by



and



C_2H_2 then can be efficiently formed from CH_4 , and the neutral-neutral reaction between C_2H_2 and CN seems to occur. The chemical model calculation supports our conclusion derived from our observations. Chapman et al. (2009) showed that the neutral-neutral reaction between C_2H_2 and CN (Reaction (1)) proceeds under the hot core condition, and C_2H_2 is released from the grain mantle inside hot cores. Our conclusion about G28.28-0.36 is consistent with their chemical model calculation. The validity of their model calculation seems to be supported by detections of HC_5N (Green et al. 2014) and HC_7N (Taniguchi et al., *in prep.*).

We next consider a possibility that Pathway 2 is the dominant formation reaction leading to HC_3N . In this reaction, three carbon atoms are not equivalent, and the expected abundance ratios are $x : y : z$ for $[\text{H}^{13}\text{CCCN}] : [\text{HC}^{13}\text{CCN}] : [\text{HCC}^{13}\text{CN}]$, where x , y , and z are arbitrary values. In fact, Sakai et al. (2010) showed that the $[\text{C}^{13}\text{CH}]/[\text{C}^{13}\text{CCH}]$ abundance ratio is $1.6 \pm 0.1 (3\sigma)$. Fukuzawa & Osamura (1997) also demonstrated their quantum chemical calculations, and their results show that a carbon atom in HNC and a carbon atom with an unpaired electron in CCH are connected. From the above two results, the abundance ratios of HC_3N should be $[\text{H}^{13}\text{CCCN}] : [\text{HC}^{13}\text{CCN}] : [\text{HCC}^{13}\text{CN}] = 1.6 : 1.0 : x$, where x is an arbitrary value, if Pathway 2 is the main formation pathway of HC_3N . Pathway 2 cannot explain our observational results, and we conclude that the reaction between C_2H and HNC is not the primary formation pathway of HC_3N .

Pathways 3 and 4 include the ion-molecule reactions. There is a possibility that there is no significant differences in abundances among all of the ^{13}C isotopologues, when the main formation mechanism is the ion-molecule reactions (Taniguchi et al. 2016). We also consider that scrambling may occur during the processes of these ion-molecule reactions. The clear differences in abundances among the three ^{13}C isotopologues of HC_3N should not be recognized, if scrambling occurs. Hence, these ion-molecule reactions are not the main formation mechanisms of HC_3N in L1527 and G28.28-0.36.

In summary, the abundance ratios derived by our observations agree with the ratios of only Pathway 1. We thus propose that the neutral-neutral reaction between C_2H_2 and CN (Reaction (1)) dominates other formation pathways in both L1527 and G28.28-0.36. This proposal also agrees with the predicted primary formation pathway of HC_3N by chemical model calculations (Hassel et al. 2008; Chapman et al. 2009).

4.2. $^{12}\text{C}/^{13}\text{C}$ Ratios in L1527 and G28.28-0.36

The $^{12}\text{C}/^{13}\text{C}$ ratios of HC_3N in L1527 are summarized in Table 3. When we assume that the excitation temperature is 9.7 K, the $^{12}\text{C}/^{13}\text{C}$ ratios are consistent with the elemental ratio of 60 – 70 in the local interstellar medium (ISM) (Langer & Penzias 1993; Savage et al. 2002; Milam et al. 2005) within 1-sigma errors. The derived $^{12}\text{C}/^{13}\text{C}$ ratios of H^{13}CCCN and HC^{13}CCN are slightly higher than the elemental ratio in the local ISM, using the excitation temperature

Table 5. ^{13}C Isotopic Fractionation of HC_3N in Various Sources

Source	H^{13}CCCN	HC^{13}CCN	HCC^{13}CN	source type	Temperature (K)	Density (cm^{-3})
L1527	0.9 (± 0.2)	1.00	1.29 (± 0.19)	WCCC	20 – 30	$\sim 10^5$ ^c
G28.28-0.36	1.0 (± 0.2)	1.00	1.47 (± 0.17)	hot core	100 – 200	$\sim 10^6$
TMC-1 CP ^a	1.0	1.0	1.4 (± 0.2)	dark cloud	~ 10	$\sim 10^4$
Serpens South 1A ^b	0.91 (± 0.09)	1.00	1.32 (± 0.09)	IRDC	~ 15	$\sim 10^5$

NOTE—The error corresponds to one standard deviation.

^aThe ratios were derived using the column densities (Takano et al. 1998).

^bThe ratios were derived using the column densities (Li et al. 2016).

^cTakakuwa et al. (2001).

of 16.9 K. However, the ratios of these two ^{13}C isotopologues are consistent with the elemental ratio in the local ISM within 2-sigma errors. The $^{12}\text{C}/^{13}\text{C}$ ratio of HCC^{13}CN agrees with the elemental ratio of the local ISM within 1-sigma error. Therefore, the ^{13}C species of HC_3N are not significantly diluted in L1527, as well as TMC-1 CP (Takano et al. 1998).

In Table 4, the $^{12}\text{C}/^{13}\text{C}$ ratios of the three ^{13}C isotopologues in G28.28-0.36 are summarized. These $^{12}\text{C}/^{13}\text{C}$ values are lower than the elemental ratio of 60 – 70 in the local ISM, because G28.28-0.36 is located nearer the Galactic center than the Earth and L1527. The $^{12}\text{C}/^{13}\text{C}$ ratio shows a gradient with Galactic distance (D_{GC}) (Savage et al. 2002; Milam et al. 2005). We estimated the D_{GC} of G28.28-0.36 to be 5.4 kpc using the trigonometry. The $^{12}\text{C}/^{13}\text{C}$ ratios at $D_{\text{GC}} = 5.4$ kpc are derived to be 39 – 65, using the results obtained by the observations of CN, CO, and H_2CO ($^{12}\text{C}/^{13}\text{C} = 6.21(1.00)D_{\text{GC}} + 18.71(7.37)$) (Milam et al. 2005). The $^{12}\text{C}/^{13}\text{C}$ ratios of HC_3N obtained by our observations are well consistent with the estimated values at $D_{\text{GC}} = 5.4$ kpc. These suggest that ^{13}C isotopologues of HC_3N are not heavily diluted, which is in good agreement with in the local ISM.

The column densities derived by the $J = 10 - 9$ lines are lower than those derived by the $J = 9 - 8$ lines by 1.3 – 1.9 times. The explanation for the differences in the column densities between the $J = 10 - 9$ lines and $J = 9 - 8$ lines is that the spatial distribution of HC_3N shows the ring-like structure with outer strong emission peaks, which is supported by our high spatial resolution map with the Very Large Array (Taniguchi et al., *in prep.*).

4.3. Comparison of ^{13}C Isotopic Fractionation in Various Sources

We summarize ^{13}C isotopic fractionation of HC_3N in the four sources, using HC^{13}CCN as a reference, in Table 5. We also summarize the source types and their typical temperatures and densities in Table 5. We categorize these four sources into the star-forming cores (L1527 and G28.28-0.36) and the starless cores (TMC-1 CP and Serpens South 1A). We can also categorize these four sources into the low-mass star forming regions (TMC-1 CP and L1527) and the high-mass star forming regions (Serpens South 1A and G28.28-0.36). We then compare various environment in star forming regions. Although there are wide ranges of temperatures (~ 10 K – 200 K) and densities ($10^4 \text{ cm}^{-3} - 10^6 \text{ cm}^{-3}$), the ^{13}C isotopic fractionation pattern in all of the four sources show the same tendency. The abundances of H^{13}CCCN and HC^{13}CCN are comparable with each other, and HCC^{13}CN is more abundant than the others. In addition, the $[\text{HCC}^{13}\text{CN}]/[\text{HC}^{13}\text{CCN}]$ ratios are in good agreement (~ 1.3) among the four sources within 1-sigma errors. These results may imply that the neutral-neutral reaction between C_2H_2 and CN (Reaction (1)) is the universal main formation mechanism of HC_3N .

5. CONCLUSIONS

We carried out observations of the $J = 9 - 8$ and $10 - 9$ rotational transitions of the three ^{13}C isotopologues of HC_3N toward the low-mass star forming region L1527 and the high-mass star forming region G28.28-0.36 with the NRO 45-m telescope. The abundance ratios are found to be 0.9 (± 0.2) : 1.00 : 1.29 (± 0.19) (1σ) and 1.0 (± 0.2) : 1.00 : 1.47 (± 0.17) (1σ) for $[\text{H}^{13}\text{CCCN}] : [\text{HC}^{13}\text{CCN}] : [\text{HCC}^{13}\text{CN}]$ in L1527 and G28.28-0.36, respectively. Our observational results suggest that the neutral-neutral reaction between C_2H_2 and CN seem to overwhelm the other formation pathways in both L1527 and G28.28-0.36. In addition, the ^{13}C isotopic fractionation pattern seen in the two star-forming regions is the same one in starless cores. The primary formation pathway of HC_3N may be common from low-mass prestellar cores to high-mass star-forming cores.

We would like to express our great thanks to the staff of the Nobeyama Radio Observatory. The Nobeyama Radio Observatory is a branch of the National Astronomical Observatory of Japan, National Institutes of Natural Sciences. In particular, we deeply appreciate Dr. Tetsuhiro Minamidani, Ms. Chieko Miyazawa, and Dr. Hiroyuki Nishitani for immediate responding to the equipment problems. We express our thanks to Mr. Mitsuhiro Matsuo (Ph. D student of Kagoshima University) for helping observations at Nobeyama. This work was supported in part by the Center for the Promotion of Integrated Sciences (CPIS) of SOKENDAI.

REFERENCES

- Aikawa, Y., Wakelman, V., Garrod, R. T., & Herbst, E. 2008, *ApJ*, 674, 993
- Chapman, J. F., Millar, T. J., Wardle, M., Burton, M. G., & Walsh, A. J. 2009, *MNRAS*, 394, 221
- Deleon, R. L., & Muentner, J. S. 1985, *JChPh*, 82, 1702
- Fukuzawa, K., & Osamura, Y. 1997, *ApJ*, 489, 113
- Garrod, R. T., & Herbst, E. 2006, *A&A*, 457, 927
- Green., C. -E., Green., J. A., Burton, M. G., et al. 2014, *MNRAS*, 443, 2252
- Hassel, G. E., Herbst, E., & Garrod, R. T. 2008, *ApJ*, 681, 1385
- Langer, W. D., & Penzias, A. A. 1993, *ApJ*, 408, 539
- Li, J., Shen, Z., Wang, J., et al. 2016, *ApJ*, 824, 136
- McElroy, D., Walsh, C., Markwick, A. J., et al. 2013, *A&A*, 550, A36
- Milam, S. N., Savage, C., Brewster, M. A., Ziurys, L. M., & Wyckoff, S. 2005, *ApJ*, 634, 1126
- Müller, H. S. P., Schlöder, F., Stutzki, J., & Winnewisser, G. 2005, *JMoSt*, 742, 215
- Purcell, C. R., Balasubramanyam, R., Burton, M. G., et al 2006, *MNRAS*, 367, 553
- Sakai, N., Sakai, T., Hirota, T., & Yamamoto, S. 2008, *ApJ*, 672, 371
- Sakai, N., Sakai, T., Hirota, T., & Yamamoto, S. 2009, *ApJ*, 702, 1025
- Sakai, N., Saruwatari, O., Sakai, T., Takano, S., & Yamamoto, S. 2010, *A&A*, 512, A31
- Savage, C., Apponi, A. J., Ziurys, L. M., & Wyckoff, S. 2002, *ApJ*, 578, 211
- Suzuki, H., Yamamoto, S., Ohishi, M., et al. 1992, *ApJ*, 392, 551
- Takakuwa, S., Kawaguchi, K., Mikami, H., & Saito, M. 2001, *PASJ*, 53, 251
- Takano, S., Masuda, A., Hirahara, Y., et al. 1998, *A&A*, 329, 1156
- Taniguchi, K., Ozeki, H., Saito, M., et al. 2016, *ApJ*, 817, 147